Integrated Optical Memory Based on Laser-Written Waveguides

Giacomo Corrielli,[1] Alessandro Seri,[2] Margherita Mazzera,[2,*] Roberto Osellame,[1] and Hugues de Riedmatten[2,3]

[1]*Istituto di Fotonica e Nanotecnologie–Consiglio Nazionale delle Ricerche and Dipartimento di Fisica–Politecnico di Milano, P.zza Leonardo da Vinci 32, 20133 Milano, Italia*

[2]*ICFO-Institut de Ciencies Fotoniques, The Barcelona Institute of Technology, 08860 Castelldefels (Barcelona), Spain*

[3]*ICREA-Institució Catalana de Recerca i Estudis Avançats, 08015 Barcelona, Spain*

(Received 10 February 2016; published 18 May 2016)

We propose and demonstrate a physical platform for the realization of integrated photonic memories based on laser-written waveguides in rare-earth-doped crystals. Using femtosecond-laser micromachining, we fabricate waveguides in $Pr^{3+}:Y_2SiO_5$ crystal. We demonstrate that the waveguide inscription does not affect the coherence properties of the material and that the light confinement in the waveguide increases the interaction with the active ions by a factor of 6. We also demonstrate that analogous to the bulk crystals, we can operate the optical pumping protocols necessary to prepare the population in atomic-frequency combs that we use to demonstrate light storage in excited and spin states of the Praseodymium ions. Our results represent a realization of laser-written waveguides in a $Pr^{3+}:Y_2SiO_5$ crystal and an implementation of an integrated on-demand spin-wave optical memory. They open perspectives for integrated quantum memories.

DOI: 10.1103/PhysRevApplied.5.054013

I. INTRODUCTION

Quantum memories (QMs) are important devices in quantum-information science. They provide an interface between flying and stationary quantum bits and are at the heart of several applications including quantum-information networks [1], quantum repeaters [2], linear optics quantum computing [3], and multiphoton quantum light sources [4]. Several QM demonstrations have been reported recently in atomic and solid-state systems [2,5,6]. In order to progress towards large-scale quantum-information architectures involving several QMs, it is important to rely on devices that can be easily duplicated and integrated. This facilitates the scalability and the realization of complex optical circuitry involving QMs. Furthermore, the tight light confinement achieved in waveguide structures leads to a strong enhancement of the light-matter interaction. Finally, the integration of QMs with other required devices, such as quantum light sources and single-photon detectors, is greatly simplified. Solid-state systems are well suited for the exploration of integrated QMs, and, in particular, rare-earth-doped solids show promising properties with bulk crystals [2,6].

Two approaches have been explored towards integrated rare-earth QMs so far. The first one is to integrate rare earths in already available systems for waveguides [7,8]. Quantum light storage has been performed in a $Ti^{4+}:Tm^{3+}:LiNbO_3$ waveguide fabricated by Ti^{4+} in-diffusion [9], where also more recently an integrated processor has been implemented [10]. These demonstrations are limited to the mapping of the light field into optical atomic excitations. Moveover, the $LiNbO_3$ matrix, although suitable for waveguide fabrication, degrades the coherence properties of the rare-earth ions, which then limits the storage performance, e.g., in terms of storage times [9]. The second approach consists of realizing waveguides in crystals already used for demonstrating bulk QM and suitable for long-term storage of quantum information, e.g., Y_2SiO_5. Photonic-crystal waveguides and cavities have been fabricated in $Nd^{3+}:Y_2SiO_5$ and $Er^{3+}:Y_2SiO_5$ using focused-ion-beam milling [11]. It was shown that the coherence properties of the rare-earth ions are preserved during the fabrication process, which is very promising for quantum applications. This fabrication technique is, however, challenging to extend to millimeter-long waveguides, which may be useful to achieve high storage and retrieval efficiencies. Also, the ions used so far possess only twofold ground states, which restricts the storage of light to the excited state, strongly limiting the achievable storage times. In order to attain spin-state storage, which enables long-term storage and on-demand read-out, ions with a threefold ground state, such as Eu^{3+} or Pr^{3+}, should be used [12–15]. $Pr^{3+}:Y_2SiO_5$ crystals are currently one of the best systems for quantum memory applications. Very efficient storage of weak coherent states [16] has been demonstrated in this material, as well as an extremely long storage time, of the order of 1 min for classical images [17]. Recently, a demonstration of an on-demand quantum memory for time-bin qubits [15] has been reported using this crystal. The coherence properties of devices based on TeO_2 slab waveguides deposited on a $Pr^{3+}:Y_2SiO_5$ crystal have been

*margherita.mazzera@icfo.es

 © 2016 American Physical Society

measured to be consistent with those of bulk ions [18], which is promising for the implementation of integrated rare-earth-based quantum devices. Nevertheless, in such a system, the active ions are only evanescently coupled to the waveguide.

Here, we propose an alternative way to fabricate waveguides in $Pr^{3+}:Y_2SiO_5$ using femtosecond-laser micromachining (FLM), where the active ions are directly coupled to the light. FLM has been demonstrated in the past two decades to be a very powerful technology for the direct inscription of high-quality optical waveguides in the bulk of both amorphous and crystalline transparent substrates [19–22]. Several complex integrated photonic devices have been developed with this technique, ranging from all-optical routers [23] and power dividers [24] to modulators [25] and frequency converters [26,27]. Moreover, it has been shown that laser-written waveguide circuits in glass are suitable for supporting the propagation of photonic qubits [28] and represent a promising platform for the development of the rapidly growing field of integrated quantum photonics [29–31]. The class of materials where waveguide writing with FLM has been demonstrated includes several rare-earth-doped crystals, e.g., Nd:YAG, Yb:YAG, Nd:YVO_4, and Pr:YLF among others, with applications mainly oriented towards the realization of integrated laser sources [32–35]. At the best of our knowledge, FLM in $Pr^{3+}:Y_2SiO_5$ crystals has never been reported in the literature before, despite it would allow us to take advantage of the direct access to the active ions and the exceptional performance as a light-storage medium.

In this paper, we demonstrate that the coherence properties of Pr^{3+} ions in femtosecond-laser-written waveguides are not affected by the fabrication procedure. We show that the light confinement in the waveguide improves significantly the interaction with the active ions. Finally, we perform storage and retrieval of light pulses using the atomic-frequency-comb (AFC) protocol both in the excited state and spin-states, demonstrating an on-demand integrated optical memory.

II. EXPERIMENT SETUP AND FABRICATION

The substrate used is a $Pr^{3+}:Y_2SiO_5$ bulk crystal (Scientific Material), 10 mm long (along the crystal b axis) and with a concentration of active ions of 0.05%. Optical waveguides are fabricated by FLM adopting the so-called type II configuration [36], where the femtosecond-laser irradiation is used to directly inscribe into the substrate two closely spaced damage tracks, in correspondence of which the material locally expands and becomes amorphous. This procedure gives rise to the formation of a stress field in their proximity, which, in turn, causes a material refractive-index alteration. By tailoring properly the irradiation parameters and geometry, it is possible with this method to obtain a light-guiding region with positive refractive-index change localized between the two tracks. It is worth highlighting that in type II waveguides, the core region (where most of the light remains confined) is only marginally affected by the fabrication process, hence, preserving all its bulk properties. Single-mode waveguides for 606-nm light are fabricated accordingly by inscribing pairs of damage tracks with a reciprocal distance of 25 μm and buried 100 μm beneath the sample top surface. Each track is fabricated by focusing a femtosecond-laser beam (a homemade Yb:KYW oscillator, $\lambda = 1030$ nm, pulse duration $\tau = 300$ fs [37]) inside the crystal volume, with optimized irradiation parameters: energy per pulse of 570 nJ, repetition rate of 20 kHz, uniform sample translation along the b axis at the speed of 57 μm/s. A microscope objective with $50\times$ magnification and 0.6 numerical aperture is used as focusing optics. Note that for higher laser repetition rates and equal energy deposited per unit volume (at a fixed pulse energy), we observe the formation of periodic disruptions along the damage tracks [38], which degrade the waveguide homogeneity and increase significantly the waveguide propagation losses. During the fabrication, the crystal orientation is such that the femtosecond-pulsed laser beam is parallel to the D_1 axis. The resulting waveguides support only one polarization mode, with the electric field oscillating parallel to the D_2 axis, which is compatible with the memory protocols, as it is the one that maximizes the interaction between the Pr^{3+} ions and the light field resonant to their ${}^3H_4(0) \rightarrow {}^1D_2(0)$ optical transition at 606 nm [39].

Our laser source at 606 nm, a second-harmonic generation laser (Toptica, DL SHG pro), is stabilized in frequency by the Pound-Drever-Hall technique to a Fabry-Perot cavity hosted in a homemade vacuum chamber [40]. Both the amplitude and the frequency are modulated with a double-pass acousto-optic modulator driven by an arbitrary waveform generator (Signadyne). We use the same beam for both memory preparation and input light pulses. After the acousto-optic modulator, the beam is steered to a separated optical table hosting the cryostat (closed-cycle cryocooler, Oxford Instruments) where the waveguide sample is fixed and maintained at a temperature of about 3 K. The coupling of the light into the waveguide is done by means of an external 75-mm focal length lens assembled in a translation stage. The final e^{-2} diameter of the beam at the waveguide input facet is 28.3 μm. After the waveguide, the light is recollected with a 100-mm focal length lens and sent to a photodetector (or CCD camera) placed at a distance of about 180 cm from the collecting lens.

III. OPTICAL MEASUREMENTS

Figure 1(a) shows a microscope picture of the waveguide cross section, in which the two damages are clearly visible. The mode supported by the waveguide, when it is coupled with 606-nm light polarized parallel to the Y_2SiO_5 crystalline D_2 axis is reported in Fig. 1(b). From the horizontal and vertical intensity profiles shown in Figs. 1(c) and 1(d), respectively, we estimate the FWHM of the guided mode to

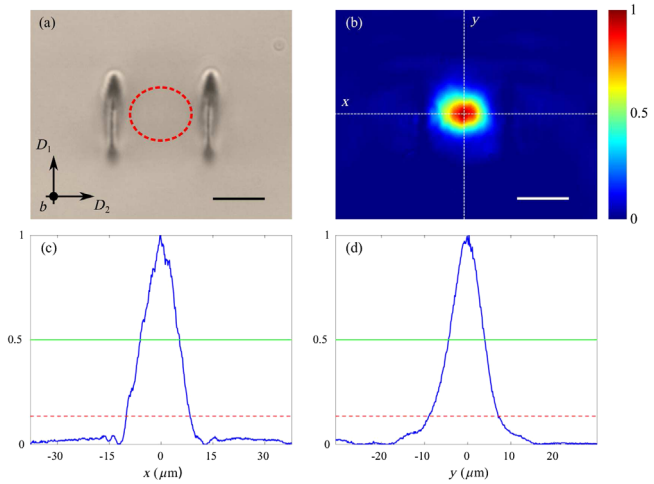

FIG. 1. (a) Microscope picture of the waveguide cross section. The distance between the damage tracks is 25 μm. The red dashed ellipse indicates the e^{-2} contour of the guided mode. Scale bar is 15 μm. (b) CCD-acquired near-field intensity profile of the guided mode. Scale bar is 15 μm. (c),(d) Normalized intensity profiles of the waveguide mode along the x and y sections indicated in panel (b). The resulting full widths at half maximum (FWHM) are $\Delta_x = 11.3$ μm and $\Delta_y = 8.6$ μm (green solid level). The measured e^{-2} diameters are $\tau_x = 18.5$ μm and $\tau_y = 15.8$ μm (red dashed level).

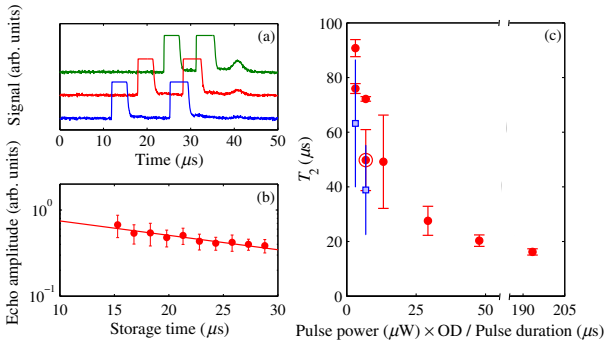

FIG. 2. (a) Pulse sequence for the two-pulse photon-echo experiment. (b) Echo efficiency as a function of the time delay 2τ. The fitting of the experimental data to an exponential decay is also shown (solid line). For this set of data, an optical coherence time $T_2 = 49.9$ μs is extrapolated. (c) Optical coherence times T_2 measured in the waveguide (circles) and in an equivalent bulk sample (squares) as a function of the quantity $[(P_p \times \mathrm{OD})/t_p]$. The circled data point in panel (c) refers to the decay shown in panel (b).

be $\Delta_x = 11.3$ μm and $\Delta_y = 8.6$ μm. The transmission of the light through the optical waveguide is about $\eta_T = 50\%$, which includes the coupling mode mismatch and waveguide propagation loss. Fresnel losses at the waveguide input and output facets are quenched by a specific antireflection coating. By rotating the polarization of 90°, the spot almost disappears, which confirms that the light is guided through the waveguide. As a matter of fact, in a bulk crystal, the polarization perpendicular to the D_2 axis will only weakly interact with the Pr^{3+} ions, experiencing a higher transmission through the sample.

To probe the coherence properties of the material after the waveguide fabrication, we perform two-pulse photon-echo experiments and measure the optical coherence time T_2. The pulse sequence used is shown in Fig. 2(a). It starts with an input pulse resonant with the $1/2_g \rightarrow 3/2_e$ transition between the ground $^3H_4(0)$ and excited $^1D_2(0)$ manifold of Pr^{3+} [see level scheme in Fig. 4(a)], which creates a coherent superposition of atomic excitations. A subsequent π pulse after a time τ is used to refocus the dipoles associated to the collective excitation and induces, thus, the so-called photon echo after a time 2τ. When the time delay τ is increased, the amplitude of the echo is reduced due to the atomic decoherence. We, thus, estimate the optical coherence time T_2 from the decay of the echo efficiency [Fig. 2(b)]. We measure T_2 in single-class absorption features of different optical depths (ODs) on the $1/2_g \rightarrow 3/2_e$ transition [15] prepared by optical pumping and by modulating the pulse power P_p. To ensure efficient population transfer even when decreasing the pulse power, the duration of the pulses t_p is simultaneously increased, reducing their spectral bandwidth. Figure 2(c) summarizes the T_2 value obtained as a function of the quantity $[(P_p \times \mathrm{OD})/t_p]$, which gives a measure of the excitation intensity (full red circles). As expected, the less ions are excited by the pulses, the longer coherence times are obtained due to the suppression of instantaneous spectral diffusion effects [41]. It is worth noting that the obtained values agree with those, also reported in Fig. 2 (open blue squares), measured when the laser beam is shifted towards the center of the $Pr^{3+}:Y_2SiO_5$ bulk, far from the laser-written waveguide but maintaining the same focusing conditions. This agreement demonstrates that the micromachining procedure does not affect the coherence properties of the material in the spatial mode where the light is guided. We also verify that the inhomogeneous broadening of the optical transition is preserved after the waveguide fabrication. The FWHM of the transmission of the $^3H_4(0) \rightarrow {}^1D_2(0)$ optical transition of Pr^{3+} is measured to be about 20 GHz, compatible with that measured in the same bulk sample.

The strength of the interaction between the light and the active ions is associated to the Rabi frequency of the optical transition, which we measure by means of optical nutation [42]. We prepare a single-class 2.5-MHz-wide absorption feature at the frequency of the optical transition to probe $[1/2_g \rightarrow 3/2_e$ between the ground $^3H_4(0)$ and excited $^1D_2(0)$ manifold]. We then send long square resonant pulses and measure the frequency of the coherent oscillation of the atoms under the light field. For inhomogeneously broadened transition and Gaussian beam profiles, the power transmitted is expected to oscillate as $J_1(\Omega_R t)/\Omega_R t$ [42]. Figure 3(a) reports an example, where the long pulse of power $P_p \approx 2$ mW is collected at the

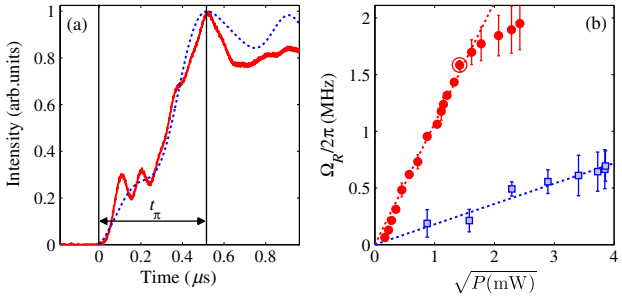

FIG. 3. (a) Intensity of a long light pulse $P_p \approx 2$ mW transmitted by a single-class absorption feature with OD $= 2.35$. The Rabi frequency $\Omega_R^{\mathrm{WG}} \approx 2\pi \times 1.6$ MHz is estimated from the rising time t_π (indicated in the figure with vertical solid lines). (b) Rabi frequency as a function of the pulse power as calculated from optical nutation measurements performed on the waveguide (circles) and on the bulk (squares). The circled data point in panel (b) refers to the pulse reported in panel (a).

photodiode after the transmission through the optical waveguide (solid curve). The pulse exhibits a fast oscillation with frequency about 10.2 MHz, i.e., the separation between the $1/2_g$ and $3/2_g$ ground states. We attribute the oscillation to beatings between the two transitions $1/2_g - 3/2_e$ and $3/2_g - 3/2_e$, which might be simultaneously excited by the pulse due to imperfect optical pumping. The Rabi frequency is calculated in a trace corrected by the fast oscillation [gray dashed curve in Fig. 3(a)] from the population inversion time t_π indicated with the dotted vertical lines, as $\Omega_R t_\pi = 5.1$. The Rabi frequencies measured for different input light powers coupled in the waveguide are shown in Fig. 3(b) as a function of the square root of the input power. For input powers up to approximately 2.6 mW, the Rabi frequency scales as the square root of the power, as expected, but at higher powers, the slope changes as if a saturation occurred. This saturation may be due to the fact that the Rabi frequency becomes comparable to the absorption feature width. Further measurements are necessary to confirm this hypothesis. When moving the beam into the bulk (black squares), the Rabi frequency increases linearly with the square root of the power with a much lower slope than that observed in the waveguide (the maximum being $\Omega_R^b \approx 2\pi \times 690$ kHz at 15 mW). For input powers at which the behavior is linear, the waveguide features light-ion interaction strengths higher than in the bulk by about a factor of 6, due to the efficient light confinement. This value agrees with that theoretically obtained (approximately 5.7) by comparing the average Rabi frequency of a beam propagating along the bulk (refractive index $n = 1.8$) focused at the input facet with our measured waist of 14 μm and of a beam confined in the waveguide with $\eta_T = 50\%$. Note that this factor can be readily increased by optimizing the mode matching and, thus, decreasing the insertion losses in the present waveguide.

IV. LIGHT STORAGE

Finally, we test our system as a storage device. The chosen storage protocol is the AFC [43]. It consists of tailoring a periodic structure, with Δ the periodicity, in a transparency window created within the inhomogeneously broadened optical transition ${}^3H_4(0) \rightarrow {}^1D_2(0)$ of Pr^{3+}. A light pulse absorbed by the structure creates a collective optical excitation which, after an initial dephasing, rephases at a time $\tau = (1/\Delta)$, giving rise to a photon-echo-like collective emission in the forward mode. Before the emission of the AFC echo, the collective optical excitation can be mapped into a spin excitation (spin wave) by applying a strong transfer pulse, effectively stopping the atomic dipole dephasing. The necessary requirement for the spin-wave storage is to have a system with three ground states, one where the AFC is prepared, one empty where the excitations are transferred, and one to use as an auxiliary state for the AFC preparation. A second transfer pulse is applied to retrieve the stored pulse. Details about the procedure to create the AFC are provided in Ref. [15]. Figure 4(a) shows the relevant level scheme of the Pr^{3+} involved in the storage with the arrows indicating the frequencies of the input and transfer pulses. In the present experiment, the ground states $1/2_g$, $3/2_g$, and $5/2_g$ are chosen as the AFC preparation, the spin-wave storage, and the auxiliary state, respectively. An example of an AFC structure with periodicity $\Delta = 400$ kHz obtained by optical pumping in the waveguide at the frequency of the $1/2_g \rightarrow 3/2_e$ transition is shown in Fig. 4(b).

The results of the AFC storage experiments performed with the waveguide are shown in Fig. 5. In Fig. 5(a), a Gaussian light pulse (FWHM $= 345$ ns) linearly polarized parallel to the D_2 axis of Y_2SiO_5 is first sent through a transparency window, about 18 MHz wide, prepared in the Pr^{3+} absorption line (black dash-dotted curves). When the polarization is rotated by 90° (black dashed curves), the light pulse at the output of the waveguide is strongly

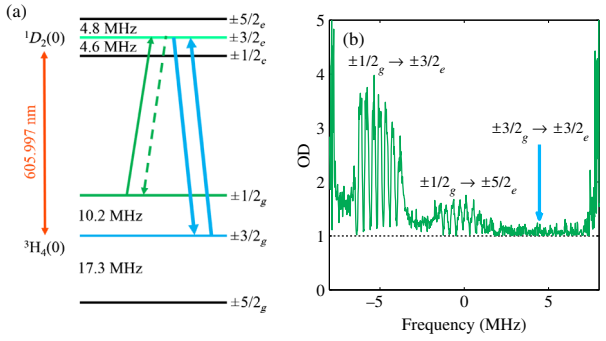

FIG. 4. (a) Energy-level scheme reporting the hyperfine separation of the lowest electronic sublevels (0) of the ${}^3H_4$ ground and ${}^1D_2$ excited manifolds of Pr^{3+} in Y_2SiO_5. The Λ scheme chosen for the storage is indicated by arrows. (b) AFC prepared at the frequency of the $1/2_g \rightarrow 3/2_e$ transition.

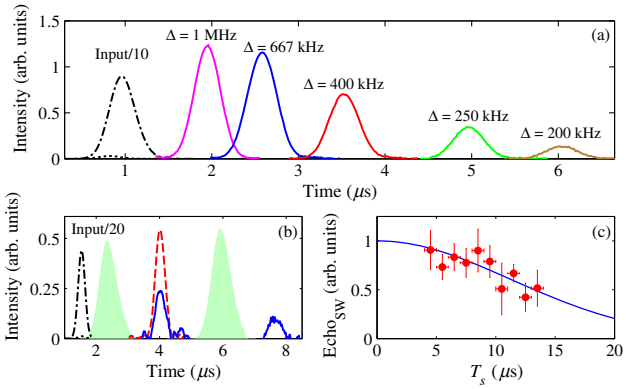

FIG. 5. Light-storage experiments using the AFC protocol. (a) Storage in excited state. Dash-dotted line: 345-ns-long input pulse transmitted through a transparency window (divided by 10 for clarity) in the absence of AFC, polarized parallel to the Y_2SiO_5 crystalline D_2 axis. Dotted line: Input pulse polarized perpendicular to the D_2 axis. Solid lines: AFC echoes for different AFC spacings Δ. (b) Spin-wave storage. Black dash-dotted curve: Similar as in (a) but 260 ns long (divided by 20 for clarity). Red dashed line: AFC echo in the absence of control pulse, at a storage time of $\tau = 2.5$ μs. The internal efficiency is $\eta_{\mathrm{AFC}} = 8.3\%$. The green plain pulses represent the control pulses, as detected before the sample by a reference detector. The blue solid line is the output when control pulses are applied, with a time difference of $T_S = 3.6$ μs. The AFC echo is partially suppressed, and a spin-wave echo appears 6.1 μs after the input. The internal efficiency of the spin-wave echo is 2%. The technical noise due to the detector is subtracted from the spin-wave storage trace. (c) Normalized spin-wave echo intensities as a function of the storage time T_S. The experimental data (dots) are fitted to a Gaussian decay to account for the inhomogeneous spin broadening from which we obtain $\gamma_{\mathrm{inh}} = (23.6 \pm 7.7)$ kHz.

suppressed [see Fig. 5(a)], as the waveguide efficiently supports only the polarization parallel to the D_2 axis. The solid lines in Fig. 5(a) correspond to the AFC echo for different AFC spacing Δ. The maximal internal storage and retrieval efficiency η_{AFC} (calculated as the ratio between the AFC echo and the input pulse transmitted through a transparency window) achieved is 14.6% for a storage time of 1.5 μs . The efficiency decreases when the storage time is increased due to a reduction of comb quality and finesse [40,43]. The device efficiency η^d_{AFC} defined as the AFC echo after the crystal divided by the input pulse before the crystal can be estimated by multiplying η_{AFC} by the waveguide transmission (50%) and by $\exp(-\mathrm{OD}_B)$, where OD_B is the background absorption in the transparency window due to imperfect optical pumping [in our case, $\mathrm{OD}_B = 1$; see dashed line in Fig. 4(b)]. We emphasize that the waveguide and background losses are not fundamental and can be significantly reduced by improving mode matching and by using shorter waveguides and/or optimized optical pumping techniques, respectively [16].

When a control pulse is applied before the rephasing of the atomic excitations, the AFC echo is partially suppressed as the transfer to the spin state takes place [see Fig. 5(b)]. After a controllable time T_s, a second control pulse is applied, and the spin-wave echo is retrieved (solid blue curve). The control pulses have a Gaussian waveform and are frequency chirped by 1.5 MHz. To confirm that the input light field is stored as a spin wave, we measure its decay when increasing the spin storage time T_s. Assuming a Gaussian decay, we extract an inhomogeneous spin broadening of $\gamma_{\mathrm{inh}} = (23.6 \pm 7.7)$ kHz compatible with those evaluated in different spin-storage experiments in $Pr^{3+}:Y_2SiO_5$ [12,13,15]. We observe an echo up to a total storage time of $t_s = 1/\Delta + T_s = 15$ μs, more than 2 orders of magnitude longer that previous AFC demonstrations (at the excited state) in waveguides [10]. The maximal internal spin-wave efficiency is $\eta_{\mathrm{SW}} = 2\%$. Similar to the storage in the excited state, waveguide and background loss have to be taken into account for estimating the device efficiency. The transfer efficiency of the control pulses is $\eta_T = 50\%$ for a laser power $P_p = 375$ μW. The transfer efficiency is estimated as $\eta_{\mathrm{SW}} = \eta_{\mathrm{AFC}} \times {\eta_T}^2 \times \eta_C$, where η_C accounts for the decoherence in the spin state and is evaluated from $\eta_T = [(\eta_{\mathrm{SW}})/\eta_{\mathrm{SW}}(0)]$, where $\eta_{\mathrm{SW}}(0)$ is the storage efficiency at $T_s = 0$. It is worth noting that the AFC and spin-wave efficiencies achieved in the waveguide sample are comparable to those obtained in similar experiments performed with weak coherent states at the single-photon level in a shorter (3 mm) $Pr^{3+}:Y_2SiO_5$ crystal [15], but the required laser power of the control beam is more than 50 times lower. The possibility to operate coherent population transfer with significantly lower power is a fundamental advantage, as the noise given by the control pulses is the main limitation for the implementation of many on-demand storage protocols at the single-photon level. Moreover, the number of atoms addressed is also decreased by the same factor, which will contribute strongly to reduce the noise. Contrary to the bulk case [15], the integrated design does not offer the possibility to spatially separate the control and echo modes (e.g., with an angle) if both propagate in the waveguide. However, a counterpropagating configuration can be adopted. Our result is, thus, very promising for the ultimate goal of extending the storage protocol to the quantum regime [14,15]. In addition, it is worth noting that an improved light-matter interaction in confined structures is also beneficial in view of observing and exploiting nonlinear effects at the single-photon level [44].

V. CONCLUSIONS

In conclusion, we demonstrate an optical memory based on laser-written waveguides in a $Pr^{3+}:Y_2SiO_5$ crystal. We show that the waveguide fabrication does not alter the coherence properties of the bulk crystal and that the light confinement in the crystal increases the light-matter interaction (as measured by the Rabi frequency) by a factor of 6 compared to a bulk crystal with the same focusing. In

addition, we report a proof-of-principle experiment of light storage using the AFC protocol. We store strong light pulses both in the excited and ground states of Pr ions. The latter represents a demonstration of an integrated on-demand spin-wave memory. These results show that integrated optical memories can be realized using laser-written waveguides, a versatile and widely used technique in integrated quantum photonics. This opens perspectives for the realization of long-lived integrated spin-wave quantum memories.

ACKNOWLEDGMENTS

We acknowledge financial support by the ERC starting grant QuLIMA, by the Spanish Ministry of Economy and Competitiveness (MINECO) and Fondo Europeo de Desarrollo Regional (FEDER) through Grant No. FIS2012-37569, by MINECO Severo Ochoa through Grant No. SEV-2015-0522 and the Ph.D. fellowship program (for A. S.), by AGAUR via 2014 SGR 1554, by the People Programme (Marie Curie Actions) of the EU FP7 under REA Grant No. 287252, by Fundació Privada Cellex, and by the European project QWAD (Grant No. FP7-ICT-2011-9-600838).

G. C. and A. S. contributed equally to this paper.

[1] H. J. Kimble, The quantum internet, Nature (London) **453**, 1023 (2008).

[2] N. Sangouard, C. Simon, H. de Riedmatten, and N. Gisin, Quantum repeaters based on atomic ensembles and linear optics, Rev. Mod. Phys. **83**, 33 (2011).

[3] E. Knill, R. Laflamme, and G. J. Milburn, A scheme for efficient quantum computation with linear optics, Nature (London) **409**, 46 (2001).

[4] J. Nunn, N. K. Langford, W. S. Kolthammer, T. F. M. Champion, M. R. Sprague, P. S. Michelberger, X.-M. Jin, D. G. England, and I. A. Walmsley, Enhancing Multiphoton Rates with Quantum Memories, Phys. Rev. Lett. **110**, 133601 (2013).

[5] A. I. Lvovsky, B. C. Sanders, and W. Tittel, Optical quantum memory, Nat. Photonics **3**, 706 (2009).

[6] F. Bussiéres, N. Sangouard, M. Afzelius, H. de Riedmatten, C. Simon, and W. Tittel, Prospective applications of optical quantum memories, J. Mod. Opt. **60**, 1519 (2013).

[7] M. U. Staudt, M. Afzelius, H. de Riedmatten, S. R. Hastings-Simon, C. Simon, R. Ricken, H. Suche, W. Sohler, and N. Gisin, Interference of Multimode Photon Echoes Generated in Spatially Separated Solid-State Atomic Ensembles, Phys. Rev. Lett. **99**, 173602 (2007).

[8] M. U. Staudt, S. R. Hastings-Simon, M. Nilsson, M. Afzelius, V. Scarani, R. Ricken, H. Suche, W. Sohler, W. Tittel, and N. Gisin, Fidelity of an Optical Memory Based on Stimulated Photon Echoes, Phys. Rev. Lett. **98**, 113601 (2007).

[9] E. Saglamyurek, N. Sinclair, J. Jin, J. A. Slater, D. Oblak, F. Bussiéres, M. George, R. Ricken, W. Sohler, and W. Tittel, Broadband waveguide quantum memory for entangled photons, Nature (London) **469**, 512 (2011).

[10] E. Saglamyurek, N. Sinclair, J. A. Slater, K. Heshami, D. Oblak, and W. Tittel, An integrated processor for photonic quantum states using a broadband light-matter interface, New J. Phys. **16**, 065019 (2014).

[11] T. Zhong, J. M. Kindem, E. Miyazono, and A. Faraon, Nanophotonic coherent light-matter interfaces based on rare-earth-doped crystals, Nat. Commun. **6**, 8206 (2015).

[12] M. Afzelius, I. Usmani, A. Amari, B. Lauritzen, A. Walther, C. Simon, N. Sangouard, J. Minár, H. de Riedmatten, N. Gisin, and S. Kröll, Demonstration of Atomic Frequency Comb Memory for Light with Spin-Wave Storage, Phys. Rev. Lett. **104**, 040503 (2010).

[13] M. Gündoğan, M. Mazzera, P. M. Ledingham, M. Cristiani, and H. de Riedmatten, Coherent storage of temporally multimode light using a spin-wave atomic frequency comb memory, New J. Phys. **15**, 045012 (2013).

[14] P. Jobez, C. Laplane, N. Timoney, N. Gisin, A. Ferrier, P. Goldner, and M. Afzelius, Coherent Spin Control at the Quantum Level in an Ensemble-Based Optical Memory, Phys. Rev. Lett. **114**, 230502 (2015).

[15] M. Gündoğan, P. M. Ledingham, K. Kutluer, M. Mazzera, and H. de Riedmatten, Solid State Spin-Wave Quantum Memory for Time-Bin Qubits, Phys. Rev. Lett. **114**, 230501 (2015).

[16] M. P. Hedges, J. J. Longdell, Y. Li, and M. J. Sellars, Efficient quantum memory for light, Nature (London) **465**, 1052 (2010).

[17] G. Heinze, C. Hubrich, and T. Halfmann, Stopped Light and Image Storage by Electromagnetically Induced Transparency up to the Regime of One Minute, Phys. Rev. Lett. **111**, 033601 (2013).

[18] S. Marzban, J. G. Bartholomew, S. Madden, K. Vu, and M. J. Sellars, Observation of Photon Echoes from Evanescently Coupled Rare-Earth Ions in a Planar Waveguide, Phys. Rev. Lett. **115**, 013601 (2015).

[19] K. M. Davis, K. Miura, N. Sugimoto, and K. Hirao, Writing waveguides in glass with a femtosecond laser, Opt. Lett. **21**, 1729 (1996).

[20] G. D. Valle, R. Osellame, and P. Laporta, Micromachining of photonic devices by femtosecond laser pulses, J. Opt. A **11**, 013001 (2009).

[21] T. Gorelik, M. Will, S. Nolte, A. Tuennermann, and U. Glatzel, Transmission electron microscopy studies of femtosecond laser induced modifications in quartz, Appl. Phys. A **76**, 309 (2003).

[22] R. R. Thomson, S. Campbell, I. J. Blewett, A. K. Kar, and D. T. Reid, Optical waveguide fabrication in *z*-cut lithium niobate ($LiNbO_3$) using femtosecond pulses in the low repetition rate regime, Appl. Phys. Lett. **88**, 111109 (2006).

[23] R. Keil, M. Heinrich, F. Dreisow, T. Pertsch, A. Tünnermann, S. Nolte, D. N. Christodoulides, and A. Szameit, All-optical routing and switching for three-dimensional photonic circuitry, Sci. Rep. **1**, 94 (2011).

[24] J. Liu, Z. Zhang, S. Chang, C. Flueraru, and C. P. Grover, Directly writing of 1-to-*N* optical waveguide power splitters in fused silica glass using a femtosecond laser, Opt. Commun. **253**, 315 (2005).

[25] Y. Liao, J. Xu, Y. Cheng, Z. Zhou, F. He, H. Sun, J. Song, X. Wang, Z. Xu, K. Sugioka *et al.*, Electro-optic integration of embedded electrodes and waveguides in $LiNbO_3$ using a femtosecond laser, Opt. Lett. **33**, 2281 (2008).

[26] R. Osellame, M. Lobino, N. Chiodo, M. Marangoni, G. Cerullo, R. Ramponi, H. T. Bookey, R. R. Thomson, N. D. Psaila, and A. K. Kar, Femtosecond laser writing of waveguides in periodically poled lithium niobate preserving the nonlinear coefficient, Appl. Phys. Lett. **90**, 241107 (2007).

[27] J. Burghoff, C. Grebing, S. Nolte, and A. Tünnermann, Efficient frequency doubling in femtosecond laser-written waveguides in lithium niobate, Appl. Phys. Lett. **89**, 081108 (2006).

[28] G. D. Marshall, A. Politi, J. C. Matthews, P. Dekker, M. Ams, M. J. Withford, and J. L. O'Brien, Laser written waveguide photonic quantum circuits, Opt. Express **17**, 12546 (2009).

[29] G. Vest, M. Rau, L. Fuchs, G. Corrielli, H. Weier, S. Nauerth, A. Crespi, R. Osellame, and H. Weinfurter, Design and evaluation of a handheld quantum key distribution sender module, IEEE J. Sel. Top. Quantum Electron. **21**, 6600607 (2015).

[30] A. Crespi, R. Osellame, R. Ramponi, D. J. Brod, E. F. Galvão, N. Spagnolo, C. Vitelli, E. Maiorino, P. Mataloni, and F. Sciarrino, Integrated multimode interferometers with arbitrary designs for photonic boson sampling, Nat. Photonics **7**, 545 (2013).

[31] M. Tillmann, B. Dakić, R. Heilmann, S. Nolte, A. Szameit, and P. Walther, Experimental boson sampling, Nat. Photonics **7**, 540 (2013).

[32] T. Calmano, J. Siebenmorgen, O. Hellmig, K. Petermann, and G. Huber, Nd:YAG waveguide laser with 1.3 W output power, fabricated by direct femtosecond laser writing, Appl. Phys. B **100**, 131 (2010).

[33] T. Calmano, J. Siebenmorgen, A.-G. Paschke, C. Fiebig, K. Paschke, G. Erbert, K. Petermann, and G. Huber, Diode pumped high power operation of a femtosecond laser inscribed Yb:YAG waveguide laser, Opt. Mater. Express **1**, 428 (2011).

[34] Y. Tan, Y. Jia, F. Chen, J. R. Vázquez de Aldana, and D. Jaque, Simultaneous dual-wavelength lasers at 1064 and 1342 nm in femtosecond-laser-written Nd: YVO_4 channel waveguides, J. Opt. Soc. Am. B **28**, 1607 (2011).

[35] S. Müller, T. Calmano, P. Metz, N.-O. Hansen, C. Kränkel, and G. Huber, Femtosecond-laser-written diode-pumped $Pr:LiYF_4$ waveguide laser, Opt. Lett. **37**, 5223 (2012).

[36] F. Chen and J. Aldana, Optical waveguides in crystalline dielectric materials produced by femtosecond-laser micromachining, Laser Photonics Rev. **8**, 251 (2014).

[37] A. Killi, U. Morgner, M. J. Lederer, and D. Kopf, Diode-pumped femtosecond laser oscillator with cavity dumping, Opt. Lett. **29**, 1288 (2004).

[38] S. Richter, S. Döring, F. Burmeister, F. Zimmermann, A. Tünnermann, and S. Nolte, Formation of periodic disruptions induced by heat accumulation of femtosecond laser pulses, Opt. Express **21**, 15452 (2013).

[39] Y. Sun, in *Spectroscopic Properties of Rare Earths in Optical Materials*, edited by G. Liu and B. Jacquir (Springer-Verlag, Berlin, 2005).

[40] D. Rieländer, K. Kutluer, P. M. Ledingham, M. Gündoğan, J. Fekete, M. Mazzera, and H. de Riedmatten, Quantum Storage of Heralded Single Photons in a Praseodymium-Doped Crystal, Phys. Rev. Lett. **112**, 040504 (2014).

[41] R. W. Equall, R. L. Cone, and R. M. Macfarlane, Homogeneous broadening and hyperfine structure of optical transitions in $Pr^{3+}:Y_2SiO_5$, Phys. Rev. B **52**, 3963 (1995).

[42] Y. Sun, G. M. Wang, R. L. Cone, R. W. Equall, and M. J. M. Leask, Symmetry considerations regarding light propagation and light polarization for coherent interactions with ions in crystals, Phys. Rev. B **62**, 15443 (2000).

[43] M. Afzelius, C. Simon, H. de Riedmatten, and N. Gisin, Multimode quantum memory based on atomic frequency combs, Phys. Rev. A **79**, 052329 (2009).

[44] N. Sinclair, K. Heshami, C. Deshmukh, D. Oblak, C. Simon, and W. Tittel, Cross-phase modulation of a probe stored in a waveguide for non-destructive detection of photonic qubits, arXiv:1510.01164.